Clay mineral assemblages of late Holocene turbidites in the Gaoping Submarine Canyon of the northeastern South China Sea and their responses to typhoon activities

Huang Huazhen [1], Liu Zhifei [1, *], Zhao Yulong [1], Zhao Hongchao [1], Fernandez Adrian R. [1], Colin Christophe [2], Lin Andrew Tien-Shun [3, 4]

[1] State Key Laboratory of Marine Geology, Tongji University, Shanghai 200092, China
[2] Université Paris-Saclay, CNRS, GEOPS, Orsay 91405, France
[3] Department of Earth Sciences, National Central University, Taoyuan 32001, Taiwan
[4] Carbon Storage and Geothermal Research Center, National Central University, Taoyuan 32001, Taiwan

* Corresponding author : Zhifei Liu, email address : lzhifei@tongji.edu.cn

Abstract :

Submarine canyons are the principal conduits for turbidity currents transporting sediments to the deep sea. Thus, turbidites, as sedimentary products of turbidity currents, can be used to trace sediment sources and transport processes and to reconstruct mechanisms of turbidity currents in submarine canyons during the geological past. Herein, clay mineral assemblage of late Holocene turbidites at Core MD18–3565 in the Gaoping Submarine Canyon is investigated to reveal the triggering mechanisms of turbidity currents. High-resolution grain-size analysis of typical coarse-grained layers characterized by basal erosion surface and fining-upward sequence in the core verifies their turbidity current origin. A total number of 318 such turbidite layers, covering ~30% of the total thickness (19.68 m) of the core, are recognized in the late Holocene sediments (33–3954 cal yr BP). Clay mineral assemblage of the turbidites is composed mainly of illite (52–60%) and chlorite (35–45%), with small quantities of smectite (0–5%) and kaolinite (0–4%), while clay mineral assemblage of the non-turbidite sediments (hemipelagites) is composed of approximately the same contents of illite (51–62%) and chlorite (34–43%), but with slightly higher smectite (0–10%) and kaolinite (1–6%). Despite the small differences in smectite and kaolinite contents, the provenance analysis identifies the Gaoping river as the predominant source of sediments in the turbidite layers, while the hemipelagite layers receive small amounts of sediments from the neighboring Erhjen, Tsengwen, and Pachang rivers besides the Gaoping river in southwest Taiwan. In combination with clay mineral compositions of surface sediments in the adjacent continental shelf and slope, as well as in-situ observational results by subaqueous moorings, we believe that the turbidity currents, in which the Gaoping river directly supplied clay minerals to the submarine canyon to form the turbidites, have been triggered mainly by typhoons passing through Taiwan. The frequency of turbidites generally keeps pace with long-term variations of El Niño-Southern Oscillation (ENSO) events, implying the potential modulation of ENSO on occurrences of late Holocene typhoon activities in the Western Pacific.

Highlights

► Turbidites in Gaoping Submarine Canyon mainly come from Gaoping river in SW Taiwan. ► Turbidity currents triggered by typhoons are responsible for turbidite occurrence. ► ENSO regulates the occurrence of late Holocene submarine canyon turbidity currents.

Keywords : Turbidity currents, Sediment transport, Provenance, ENSO, Southwest Taiwan

1. Introduction

Submarine canyons are the principal conduits for turbidity currents transporting sediments to the deep sea. Turbidites, as sedimentary products of turbidity currents, are believed to bear abundant information on global and regional tectonic, climatic, and sea level change histories, and are widely used to study triggering mechanisms of turbidity currents and to reconstruct paleoenvironmental changes (Piper and Normark, 2009; Zhao et al. 2011; Lombo Tombo et al., 2015; Fournier et al., 2017). The Gaoping Submarine Canyon, located off southwest Taiwan and in the northeastern South China Sea (SCS), is featured with steep topography, active seismicity, and high terrigenous sediment flux (Liu et al., 2020). In-situ observations have revealed that turbidity currents occur frequently, and typhoons passing through Taiwan are the most important factor triggering turbidity currents in the modern Gaoping Submarine

Canyon (Liu JT et al., 2006, 2009, 2012, 2013, 2016; Zhang et al., 2018). For example, two turbidity-current events broke the subsea fiber-optic telecommunication cables in the Gaoping Submarine Canyon in 2009 and 2015, respectively, and further studies have shown that they were triggered by Typhoons Morakot (2009) and Soudelor (2015) (Carter et al., 2012; Gavey et al., 2017). Zhang et al. (2018) found that 16 among a total number of 23 turbidity-current events in the Gaoping Submarine Canyon from May 2013 to October 2016 were directly linked to typhoon activities. However, few attentions have been paid to the connection between typhoon activities and turbidity currents during the pre-modern periods, i.e., the pre-instrumental period.

Turbidites are frequently recognized in sediment cores covering the past ~26 kyr, obtained from the Gaoping Submarine Canyon (Yu et al., 2017). However, it remains unclear how these turbidity currents were triggered, probably owing to the deficiency of appropriate proxies (Chiang and Yu, 2011; Su et al., 2012; Yu et al., 2017). Previous studies have shown that terrigenous sediments of typhoon-triggered turbidites are mostly derived from fluvial inputs (Zhang et al., 2018), while those of earthquake-triggered turbidites are mainly from landslides in the canyon (Gavey et al., 2017). As a result, it is likely to adopt the provenance analysis of turbidites as a potential approach to distinguish triggering mechanisms of turbidity currents occurred in the Gaoping Submarine Canyon. Therefore, our working hypothesis is that turbidity currents with sediments derived directly from the connected Gaoping river are triggered by typhoons, while those from adjacent other rivers and shelf/slope in the canyon areas are triggered by earthquakes or other mechanisms.

Clay minerals are the most important terrigenous detrital components of deep-sea sediments, and they have been widely used for provenance analysis (Liu Z et al., 2016). For example, using clay mineralogy of seafloor surface and riverine sediments, Liu et al. (2008) found that terrigenous sediments in the

northeastern SCS are mainly from South China, Taiwan, and Luzon. The high sedimentation rate and frequent turbidity currents in the Gaoping Submarine Canyon favor the deposition of turbidites, making it an ideal location for the study of turbidity-current triggering mechanisms (Chiang and Yu, 2011). In this study, Core MD18-3565 obtained from the lower reach of the Gaoping Submarine Canyon was chosen to perform clay mineral analysis and high-resolution grain-size measurement of typical turbidite layers, aiming to investigate the provenance of turbidites and triggering mechanisms of turbidity currents in the Gaoping Submarine Canyon during the late Holocene.

2. Regional background

2.1. Geological settings

The northeastern SCS is surrounded by South China, Taiwan, and Luzon, and it is connected to the East China Sea in the north through the Taiwan Strait and to the Pacific Ocean in the east through the Luzon Strait (Fig. 1A). Active continental margin, characterized by narrow shelf and steep slope, is developed to the east of the Manila Trench, while passive margin with broad shelf and gentle slope is developed at the western side. South China has been tectonically stable since the Mesozoic, with Mesozoic-Cenozoic granites and Paleozoic sedimentary rocks dominating in the east and Permian-Triassic limestones in the west (Liu et al., 2007). Lithology of Luzon is composed mostly of basaltic to andesitic volcanic rocks and pyroclastic rocks, due to intense volcanic activities over the Cenozoic (Commission for the Geological Map of the World, 1975). Taiwan is tectonically active since its formation in the late Miocene by arc-continent collision (Lin et al., 2003). The Taiwan orogenic belt is dominated by Neogene to Quaternary sedimentary rocks (mainly mudstones and sandstones), Eocene to Miocene slate, and pre-Tertiary metamorphic rocks, with the Coastal Range in the east dominated by Cenozoic volcanic rocks

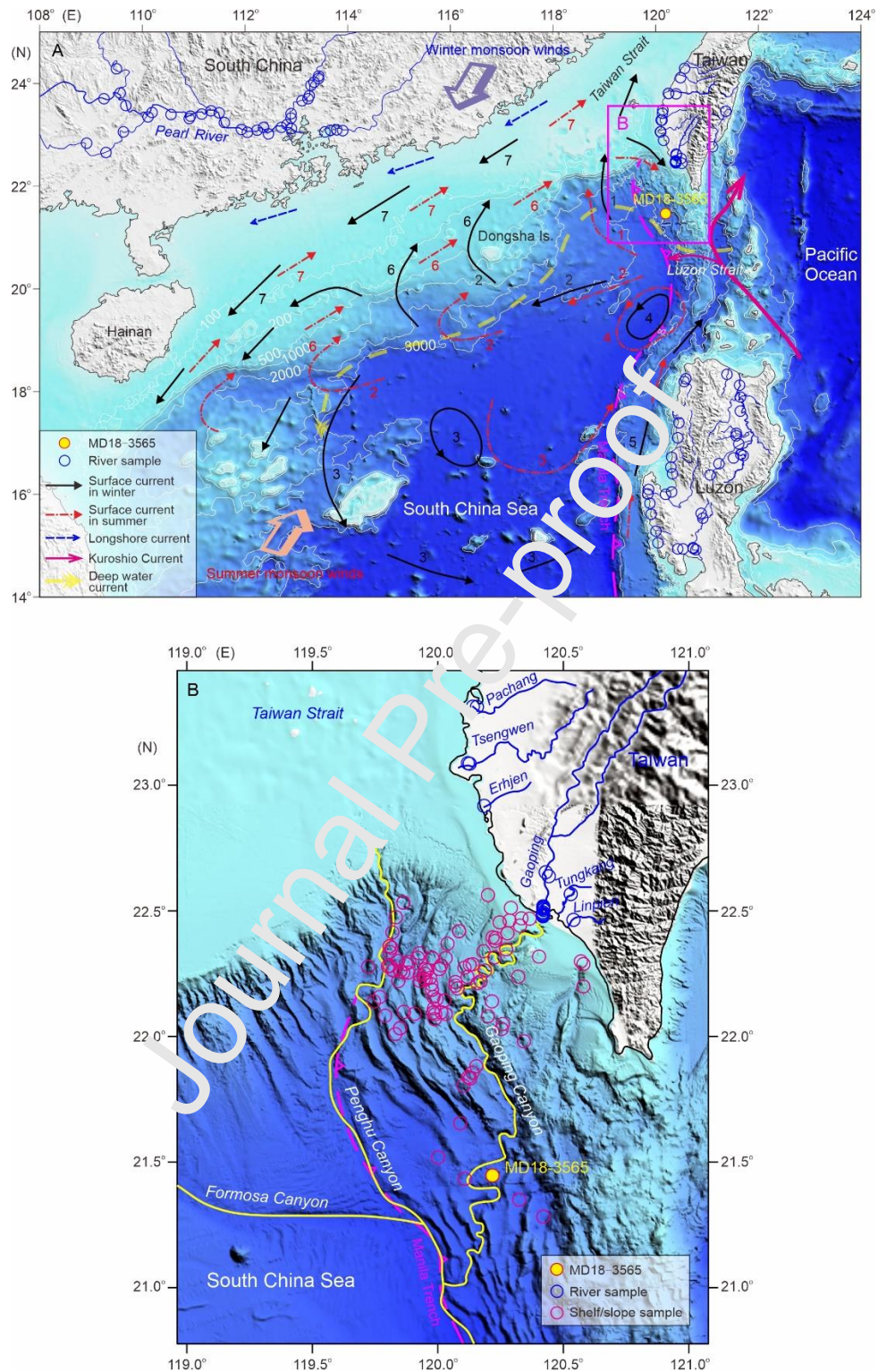and Miocene to Quaternary sediments (Huang et al., 1997).

Fig. 1. Topography and oceanography of the northeastern South China Sea (SCS). (A) Current systems and

monsoon winds in the northeast SCS and fluvial systems on surrounding continents (Liu et al., 2010).

Monsoon winds after Webster (1994); surface current after Fang et al. (1998); deep current deduced from

Qu et al. (2006); longshore current after Wang et al. (1986). Numbers for winter and summer surface currents (Fang et al., 1998): 1, Loop Current; 2, SCS Branch of Kuroshio; 3, NW Luzon Cyclonic Gyre; 4, NW Luzon Cyclonic Eddy; 5, NW Luzon Coastal Current; 6, SCS Warm Current; 7, Guangdong Coastal Current. (B) Submarine canyon systems off Southwest Taiwan, including Gaoping, Penghu, and Formosa canyons. Locations of Core MD18-3565 and referred surface sediments at surrounding river systems and on the Southwest Taiwan margin (Gaoping shelf/slope) are indicated.

2.2. Climatic and oceanographic characteristics

Climate in the northeastern SCS is modulated by the East Asian monsoon, with hot and wet climate during summer monsoon (southwesterly winds) seasons and cold and dry climate during winter monsoon (northeasterly winds) seasons (Fig. 1A). Precipitation in this region is also greatly affected by typhoon activity. A total number of 255 typhoons have passed through Taiwan in the past 60 yr, with an average of 4 typhoons per year (Liu et al., 2013). Rainfall brought by typhoon accounts for as high as 47.5% of the annual precipitation of Taiwan (Chen et al., 2010).

The currents in the northern SCS are regulated by monsoon at the surface and intrusion of Pacific water at the deep, along with the SCS branch of Kuroshio Current at the upper water column (Fig. 1A). Under influences of the alternating summer and winter monsoons, an anticyclonic gyre forms in summer and a cyclonic gyre (NW Luzon Cyclonic Gyre) exists in winter in the northern SCS (Fang et al., 1998). Forced by the persistent baroclinic pressure gradient, deep water from the North Pacific enters the SCS through the Luzon Strait, forming an anticyclonic circulation in the deep SCS (Qu et al., 2006). The Kuroshio Current enters the SCS through the Luzon Strait in the subsurface, forming the SCS branch of Kuroshio Current. This branch evolves into a clockwise circulation of warm currents (SCS Warm Current),

triggering the generation of a series of mesoscale anticyclonic eddies from south of Taiwan to west of the

Dongsha Islands (Hu et al., 2000; Caruso et al., 2006).

2.3. Physiography of the Gaoping Submarine Canyon

The Gaoping Submarine Canyon is a typical river-connected submarine canyon located off southwest

Taiwan. Upon entering the SCS, it traverses the narrow shelf and steep slope, and merged into the Manila

Trench (Fig. 1B). The canyon is approximately 260 km long, with its headwaters located <1 km from the

Gaoping river mouth. The canyon is featured by its sinuous topography, with steep walls and distinct

thalweg (the lowest part of canyon). The upper reach of the canyon has a typical V shape, and it meanders

southwesterly at the water depth range of 100–1800 m (Chiang and Yu, 2006). The middle reach of the

canyon ranges from 1800 to 2600 m water depth. It extends to the southeast and is relatively straight, with

an incised depth of 500–700 m from both sides of levees. The lower reach has a U-shaped cross section,

with an incised depth of only 200–300 m from levees. It occupies the 2600–3600 m water depth range of

the canyon, and eventually merged into the Manila Trench.

2.4. Riverine sediment inputs to the northeastern SCS

The northeastern SCS receives a huge amount of terrigenous sediments from South China, Taiwan,

and Luzon (Fig. 1A). Rivers from South China supply annually 102 Mt of sediments to the SCS (Milliman

and Farnworth, 2011), while the annual discharge of Luzon rivers is ~13 Mt (Liu Z et al., 2009). Due to

strong tectonic activities and heavy rainfall, Taiwan is the most prominent sediment source for the northern

SCS. Sediment discharge of six small mountainous rivers draining southwest Taiwan, including Linpien,

Tungkang, Gaoping, Erhjen, Tsengwen, and Pachang rivers, reaches 115.4 Mt/yr (Dadson et al., 2003; Fig.

1B; Table 1). The Gaoping river, the second longest river in Taiwan, alone provides 49 Mt/yr of fluvial

sediments to the SCS, with the overwhelming majority transported via the Gaoping Submarine Canyon.

The Erhjen and Tsengwen rivers follow with 30 Mt/yr and 25 Mt/yr, respectively.

Table 1. Drainage area, runoff, and suspended sediment discharge of major rivers in southwest Taiwan

(Dadson et al., 2003).

River name	Drainage area (km^2)	Runoff (mm/yr)	Suspended sediment discharge (Mt/yr)
Pachang	441	1500	6.3
Tsengwen	1157	1100	25.1
Erhjen	175	1800	30.3
Gaoping	3076	2500	49.0
Tungkang	175	2900	0.4
Linpien	310	2500	3.3

3. Material and Methods

3.1. Material

Core MD18-3565 (21º26.48' N, 120º12.57' E, 2697 m water depth; Fig. 1B), with a total length of

19.68 m, was collected from a sandbar in the lower reach of the Gaoping Submarine Canyon during the

HydroSed cruise of R/V *Marion Dufresne* in 2018 (Colin et al., 2018). The core is composed mainly of

gray muddy sediments, interbedded with multiple centimeter-scale coarse-grained layers of gray sandy silts

and silty sands (Fig. 2). The coarse-grained layers are featured by erosion surface at the bottom and

fining-upward sequence, and are thus recognized as turbidite layers visually at the lithology description

stage (e.g., Shanmugam, 1997). Based on detailed statistics from high-resolution core photographs, 318

turbidite layers are identified in Core MD18-3565 (Fig. 2; Supplementary data Table S1). The total

thickness of all turbidite layers reaches 581 cm, accounting for ~30% of the total core length. Thickness of

the individual layer varies from 0.1 to 27.2 cm, with an average thickness of 1.8 cm. The turbidite layers are more frequent and relatively thicker in the upper and lower parts of the core, and less frequent and relatively thinner in the middle.

The entire core sessions were collected at a depth resolution of 10 cm to obtain 197 samples for clay mineral analysis, with 54 samples collected in the turbidite layers and 143 samples in non-turbidite (hemipelagite) sediments. Two typical coarse-grained layers (one for sandy silt layer at depth interval 13.51–13.69 m and the other for silty sand layer at depth interval 18.53–18.97 m) were collected at a resolution of 1 cm to obtain 54 samples for grain size analysis in order to verify their turbidity current origin. In addition, 8 samples were collected from the hemipelagites to perform AMS ^{14}C dating of planktonic foraminifers.
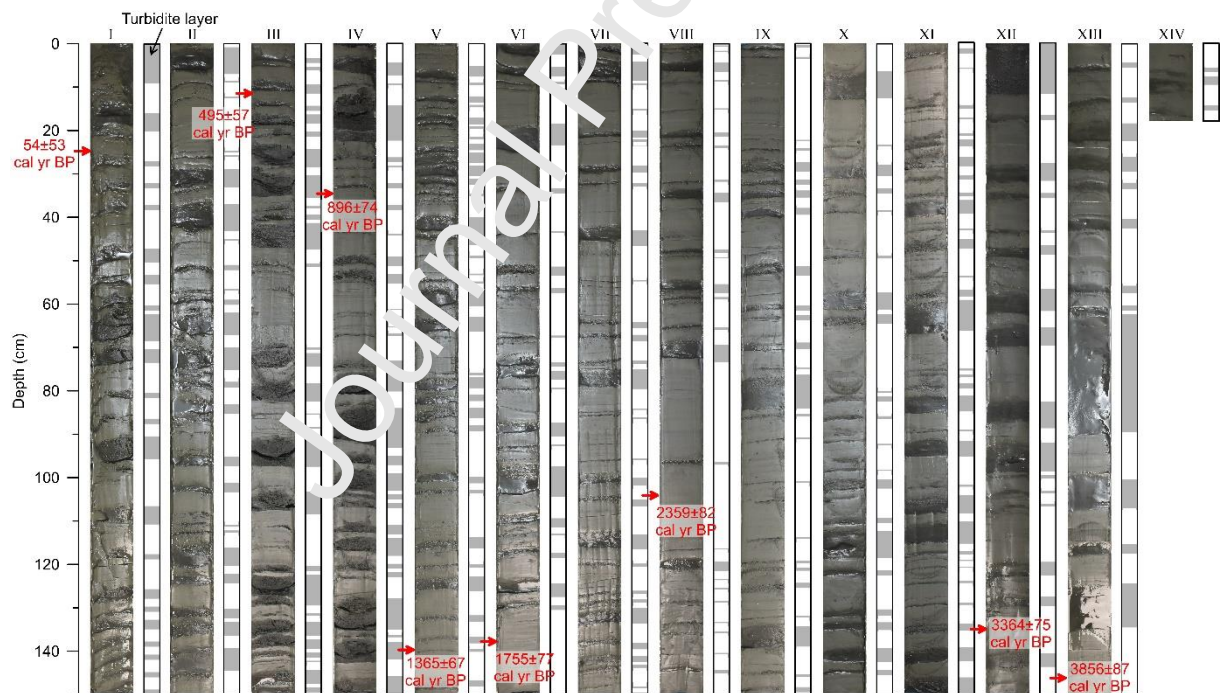

Fig. 2. Core photos and observable turbidite layers (gray bands) of Core MD18-3565 in the Gaoping Submarine Canyon. AMS ^{14}C dates (Table 2) of planktonic foraminifers and their positions at core sections are indicated. Core photos edited from Colin et al. (2018).

3.2. Methods

Clay minerals were identified by X-ray diffraction (XRD) on oriented mounts of clay-sized (<2 μm) fractions at the *State Key Laboratory of Marine Geology, Tongji University*. The pretreatment of bulk samples was performed following the methods described in Liu et al. (2003, 2004). The bulk samples were in turn reacted with 10% hydrogen peroxide (H_2O_2) and 0.5% hydrochloric acid (HCl) to remove biogenic organic matters and carbonates, respectively. The mixtures were then rinsed repeatedly with deionized water until the solution became neutral. The clay-sized (<2 μm) fractions were extracted following the Stokes' Law of Particle Settling and centrifuged to separate water. The oriented mounts of clay minerals were made by smearing the sediments in a 1-mm deep thin depression of the thin slides. The samples were measured using a PANalytical X'Pert PRO diffractometer, under conditions of 45 kV voltage and 40 mA intensity, using CuKα radiation and Ni filter. For each sample, XRD measurements were performed respectively on air-dried, ethylene-glycol saturated (24 hr), and heated (490ºC for 2 hr) conditions.

Identification of clay minerals was based on the basal reflections of the XRD diagrams (Liu et al., 2003, 2004). Contents of each group of clay minerals were calculated based on semi-quantitative estimation of area ratios of the 17 Å (001 peak of smectite), 10 Å (001 peak of illite), and 7 Å (doublet 001 peak of kaolinite and 002 peak of chlorite) peaks of glycolated curves, using the MacDiff software (Petschick, 2000; Fig. 3). Relative proportions of kaolinite and chlorite were determined based on the area ratios of 3.57 Å (002 peak of kaolinite) and 3.53 Å (004 peak of chlorite) doublet peaks (Guo and Underwood, 2011). Illite crystallinity was calculated as half height width of the 10 Å peak. The weighting factors introduced by Biscaye (1965) were not used when calculating relative percentages of each clay mineral, considering their uncertainty (Gensac, 2008; Kahle et al., 2002; Liu et al., 2010). Replicate analysis of selected samples gave a precision of ±2% (2σ), and the semi-quantitative evaluation of clay

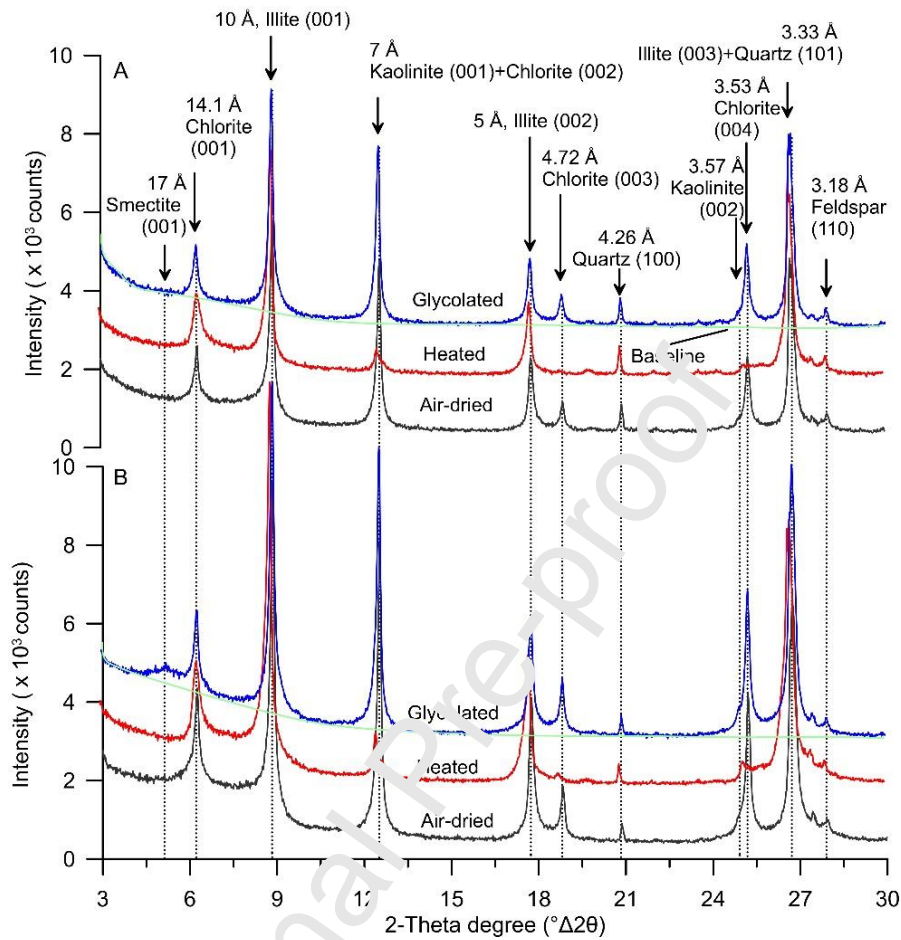mineral has an accuracy of ~5% (Liu Z et al., 2016).

Fig. 3. Multiple X-ray diffractograms of typical samples from Core MD18-3565 in the Gaoping Submarine Canyon. (A) Turbidite sample (0.17 m in depth) without clear 17 Å and 3.57 Å peaks, indicating negligible contents of smectite and kaolinite. (B) Hemipelagite sample (1.71 m in depth) with small but clear 17 Å and 3.57 Å peaks, implying the present of small amounts of smectite and kaolinite.

Grain-size distribution of bulk terrigenous sediments (carbonate and organic-free) was analyzed using a Coulter LS-230 laser particle size analyzer at the *State Key Laboratory of Marine Geology, Tongji University*. The samples (2–3 g each) were firstly treated with 10% H_2O_2 for 3 days to eliminate organic matter. The samples were then decarbonized via complete reaction with 0.5% HCl using a magnetic stirring

apparatus (60 min). The acidified samples were then washed with distilled water several times until they

became neutral. All samples were measured twice and showed good repeatability. The analysis shows a

measuring range of 0.4–2000 μm, and replicate analysis of the sample gave a precision of ±1%. Grain size

values of mean (average grain size), D_{50} (median particle size, the portions of particles with sizes smaller

and larger than this value are 50%) and D_1 (the portion of particles with sizes below this value is 1%) were

calculated to show the vertical distributions of two typical turbidite layers.

3.3. Establishment of the chronology

The age model of Core MD18-3565 was established based on eight AMS ^{14}C dating points of

planktonic foraminifers measured at the *Beta Analytical Laboratory*, USA. The planktonic foraminifers

were mixtures of *Globigerinoides ruber*, *Globigerinoides sacculifer*, and *Globigerinoides bulloides* owing

to the insufficient specimens of individual species (Table 2). To obtain the calendar ages of the AMS ^{14}C

dates, the conventional radiocarbon ages were calibrated using the Calib software (version 8; Stuiver and

Reimer, 1993) with the Marine20 curve (Heaton et al., 2020) without a further adjustment for a regional

radiocarbon reservoir age. Before the calibration, there was an additional procedure for the first

radiocarbon age (590 ± 30 yr BP). Because the minimum valid radiocarbon age for the Marine20

calibration curve (603 yr BP, Heaton et al., 2020) was larger than 590 yr BP, we used 610 ± 10 (600–620)

yr BP to perform the calibration for the first age. The calibrated ages are listed in Table 2. Considering that

the turbidites are episodic deposits, all turbidite layers were excluded to create a new continuous sediment

sequence. The turbidite-free sequence was then interpolated using the Clam package with the default

settings (95% confidence intervals, 1000 iterations; Blaauw, 2010) to build a depth-age model. Within the

95% confidence interval, the Clam calculates the weighted mean of all calendar ages for every depth

(default 1 cm step) to find the single best depth-age result (Blaauw, 2010). Therefore, the best age-depth

result is the optimal result from the Clam age model and is used for further analysis. According to the best

age-depth result (Fig. 4), Core MD18-3565 records a time interval of 33–3954 cal yr BP with an average

sedimentation rate of 0.38 cm/yr, corresponding to the late Holocene.

Table 2. AMS ^{14}C dates of planktonic foraminifers from Core MD18-3565 in the Gaoping Submarine Canyon.

| Sample ID	Depth (cm)	Depth after removing turbidite layers (cm)	Sample material	AMS ^{14}C age (yr BP)	Calendar age (1σ) (cal yr BP)
Md01	22.0	9.0	*G. ruber, G. sacculifer, G. bulloides*	590 ± 30	54 ± 53
Md02	311.5	204.2	*G. ruber, G. sacculifer, G. bulloides*	1060 ± 30	495 ± 57
Md03	485.0	300.6	*G. ruber, G. sacculifer, G. bulloides*	1520 ± 30	896 ± 74
Md04	741.0	471.0	*G. ruber, G. sacculifer, G. bulloides*	1980 ± 30	1365 ± 67
Md05	885.0	582.2	*G. ruber, G. sacculifer, G. bulloides*	2310 ± 30	1755 ± 77
Md06	1155.0	806.3	*G. ruber, G. sacculifer, G. bulloides*	2790 ± 30	2359 ± 82
Md07	1783.0	1272.6	*G. ruber, G. sacculifer, G. bulloides*	3620 ± 30	3364 ± 75
Md08	1945.0	1367.5	*G. ruber, G. sacculifer, G. bulloides*	4020 ± 30	3856 ± 87
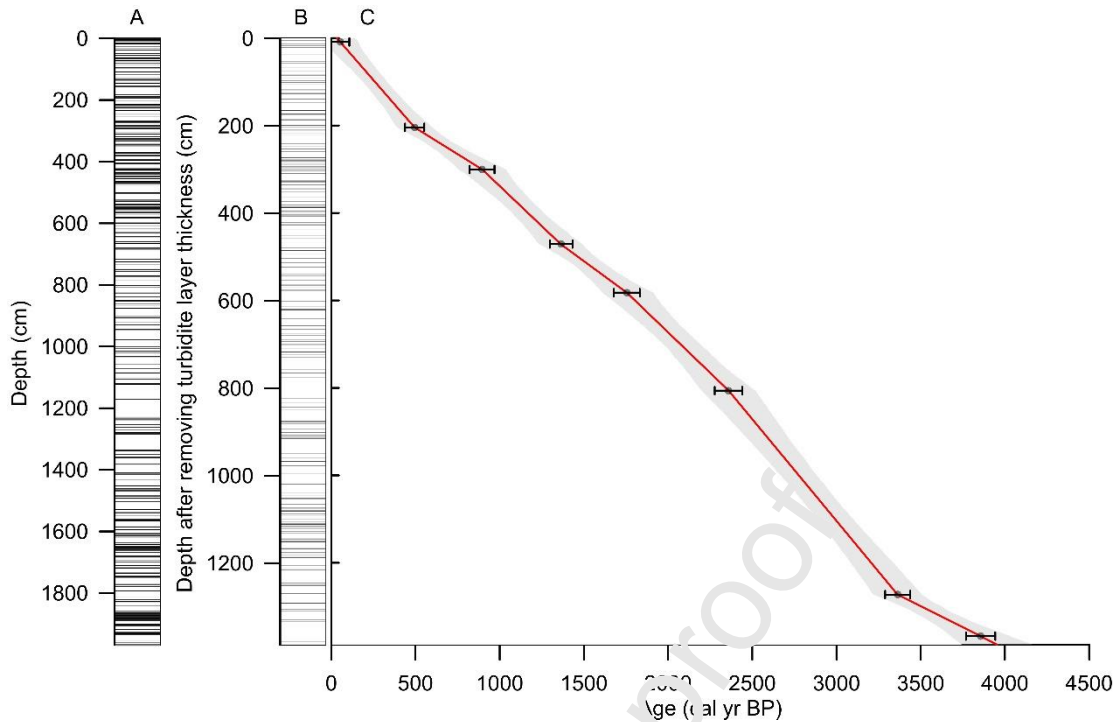
Fig. 4. Age-depth model of Core MD18-3565 in the Gaoping Submarine Canyon. (A) Turbidite layer

distribution at original core depth scale. (B) Turbidite layer distribution at depth scale after removing

turbidite layer thickness. (C) Age-depth model established using the Clam package with linear interpolation.

The red line represents the best modelling result and the gray shadow indicates the 95% confidence interval

(Blaauw, 2010).

4. Results

4.1. Clay mineral assemblages

The clay mineral assemblage of Core MD18-3565 consists mainly of illite (51–62%, average 57%)

and chlorite (34–45%, average 39%), with minor amounts of smectite (0–10%, average 2%) and kaolinite

(0–6%, average 2%) (Fig. 5, Supplementary data Table S2). The illite crystallinity varies from 0.146° to

0.210°Δ2θ, with an average of 0.164°Δ2θ. Temporal variability of the clay mineral assemblage shows that

smectite and kaolinite contents have similar trend, while illite content varies reversely (Figs. 6 and 7). The

variation of chlorite content is somewhat alike that of illite. No secular trend is observed in temporal

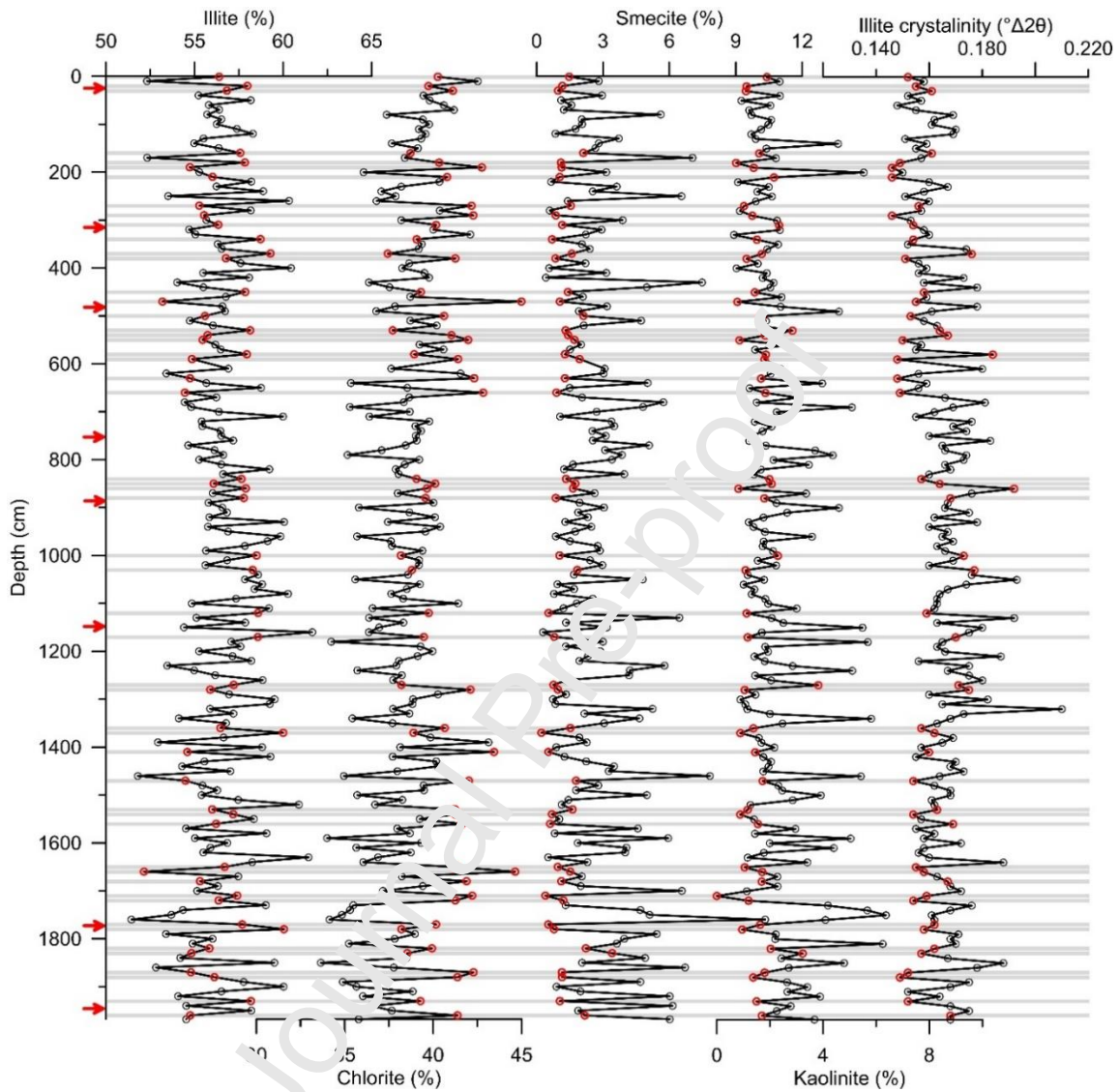variation of the clay mineral contents (Fig. 6).

Fig. 5. Depth-scale clay mineral assemblages of Core MD18-3565 in the Gaoping Submarine Canyon. Gray

bands show the occurrence of turbidite layers. Red dots represent turbidite samples. Red arrows indicate the
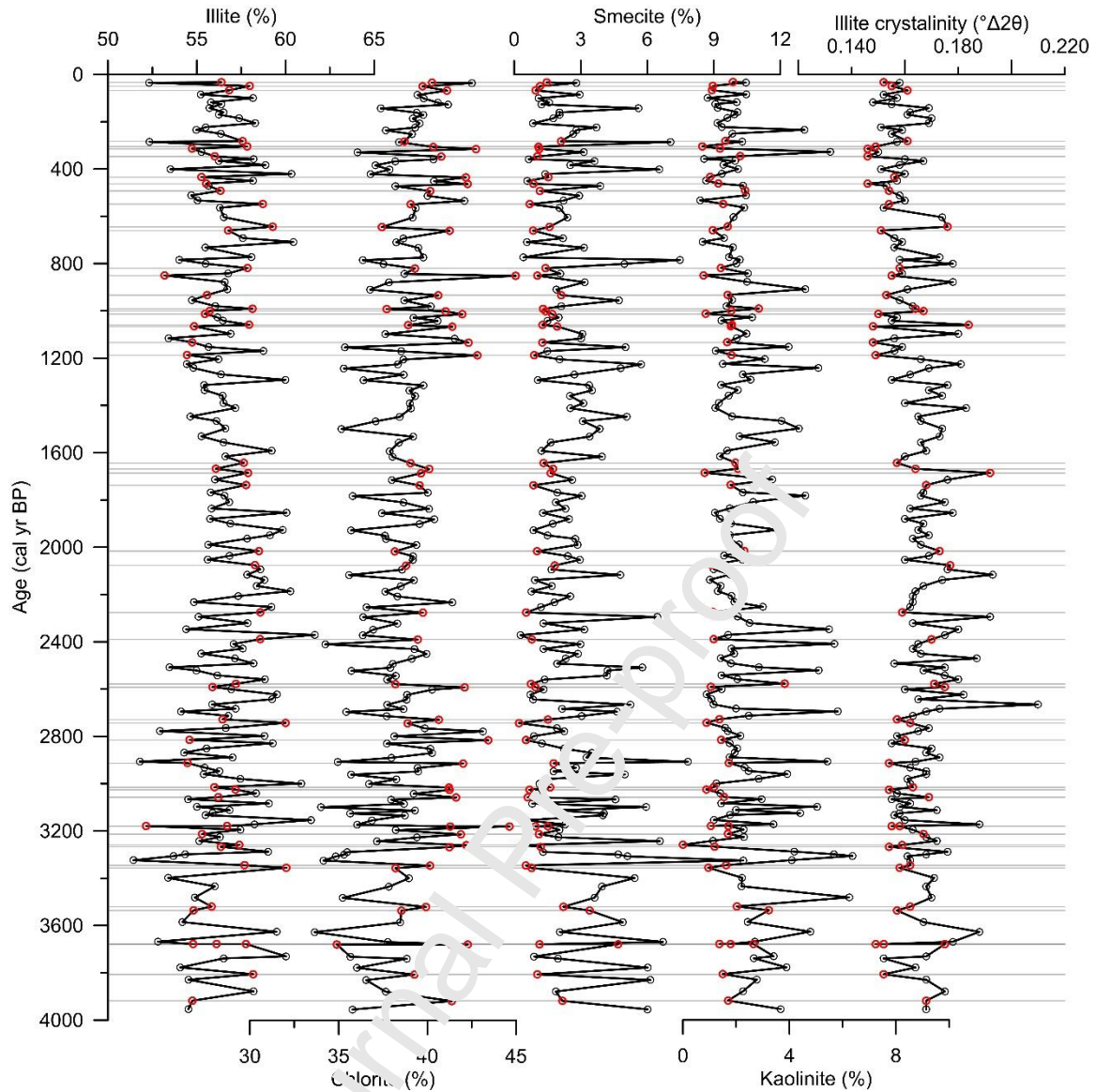
positions of AMS ^{14}C dates.

Fig. 6. Temporal variations of clay mineral assemblages of Core MD18-3565 over the past 4000 yr in the

Gaoping Submarine Canyon. Gray lines show the occurrence of turbidite layers. Red dots represent

turbidite samples.

Comparing clay mineral assemblages of the turbidites to the hemipelagites, the turbidites contain

slightly higher chlorite (35–45%, average 41 ± 1.8%), lower smectite (0–5%, average 1 ± 0.7%) and

kaolinite (0–4%, average 1 ± 0.6%), and roughly consistent illite (52–60%, average 57 ± 1.6%) (Fig. 7); the

hemipelagites contain 51–62% illite (average 57 ± 2.0%), 34–43% chlorite (average 38 ± 2.0%), 0–10%

smectite (average 3 ± 1.8%), and 1–6% kaolinite (average 2 ± 1.3%). The illite crystallinity of the turbidites

(0.146°–0.192°Δ2θ) is close to that of the hemipelagites (0.148°–0.210°Δ2θ).

Although clay mineral contents in the turbidites and hemipelagites are not much different from each

other, the discrepancy is still greater than experimental precision (±2%), and thus is statistically significant

enough to distinguish between the two types of sediments (Fig. 7).
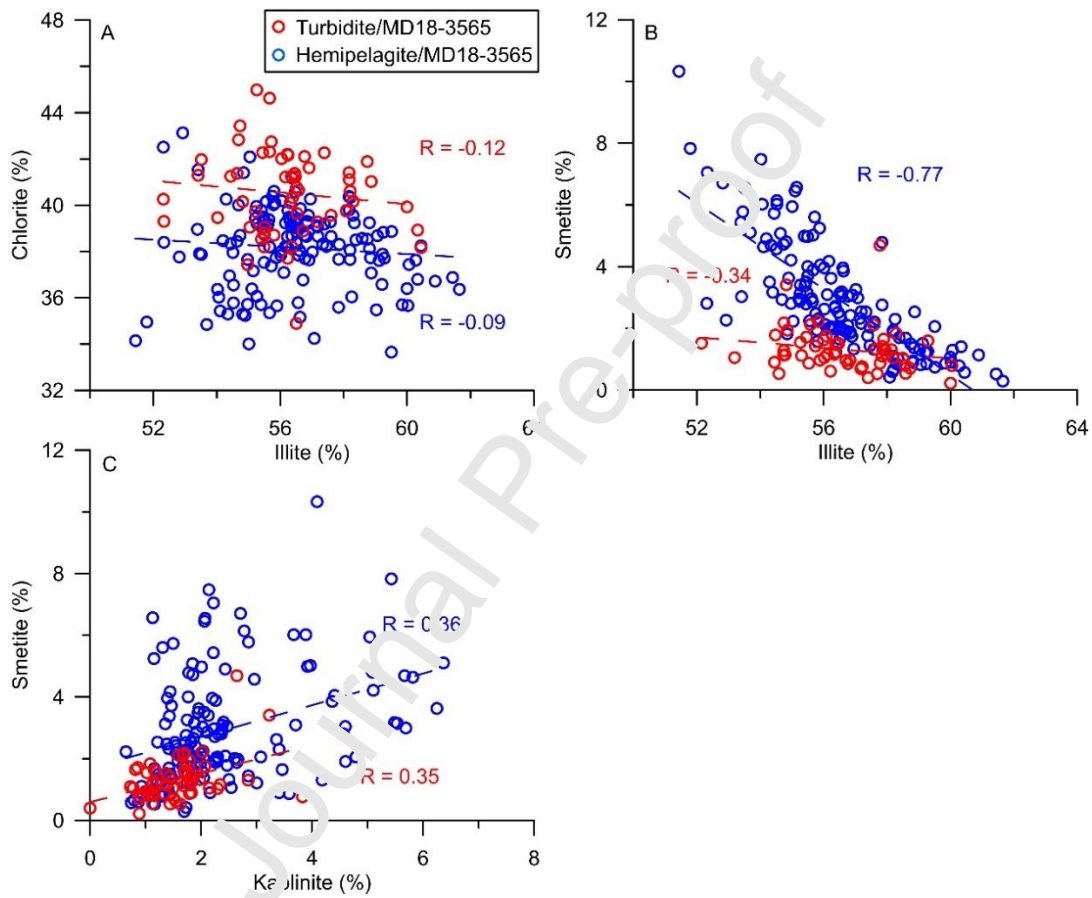

Fig. 7. Correlation plots of clay mineral groups of Core MD18-3565 in the Gaoping Submarine Canyon. (A)

Illite (%) versus chlorite (%). (B) Illite (%) versus smectite (%). (C) Kaolinite (%) versus smectite (%). Red

and blue dots represent turbidite and hemipelagite samples, respectively.

4.2. Grain size distributions

Typical coarse-grained layers of both sandy silts and silty sands show abrupt increases in all grain-size

values at their bottoms and fining-upward on the fine-grained backgrounds (Fig. 8; Supplementary data

Table S3). The sandy silt layer (Fig. 8A) presents grain size values of 32–64 μm for mean, 43–80 μm for

D_{50}, and 146–305 μm for D_1, while the silty sand layer (Fig. 8B) shows grain size values of 34–150 μm for

mean, 50–177 μm for D_{50}, and 175–543 μm for D_1. Their fine-grained backgrounds display similar

grain-size values of 6–7 μm for mean, 7–8 μm for D_{50}, and 40–48 μm for D_1. The abrupt increases in all

grain-size values are consistent with the erosion surface at the bottom of the coarse-grained layers, as

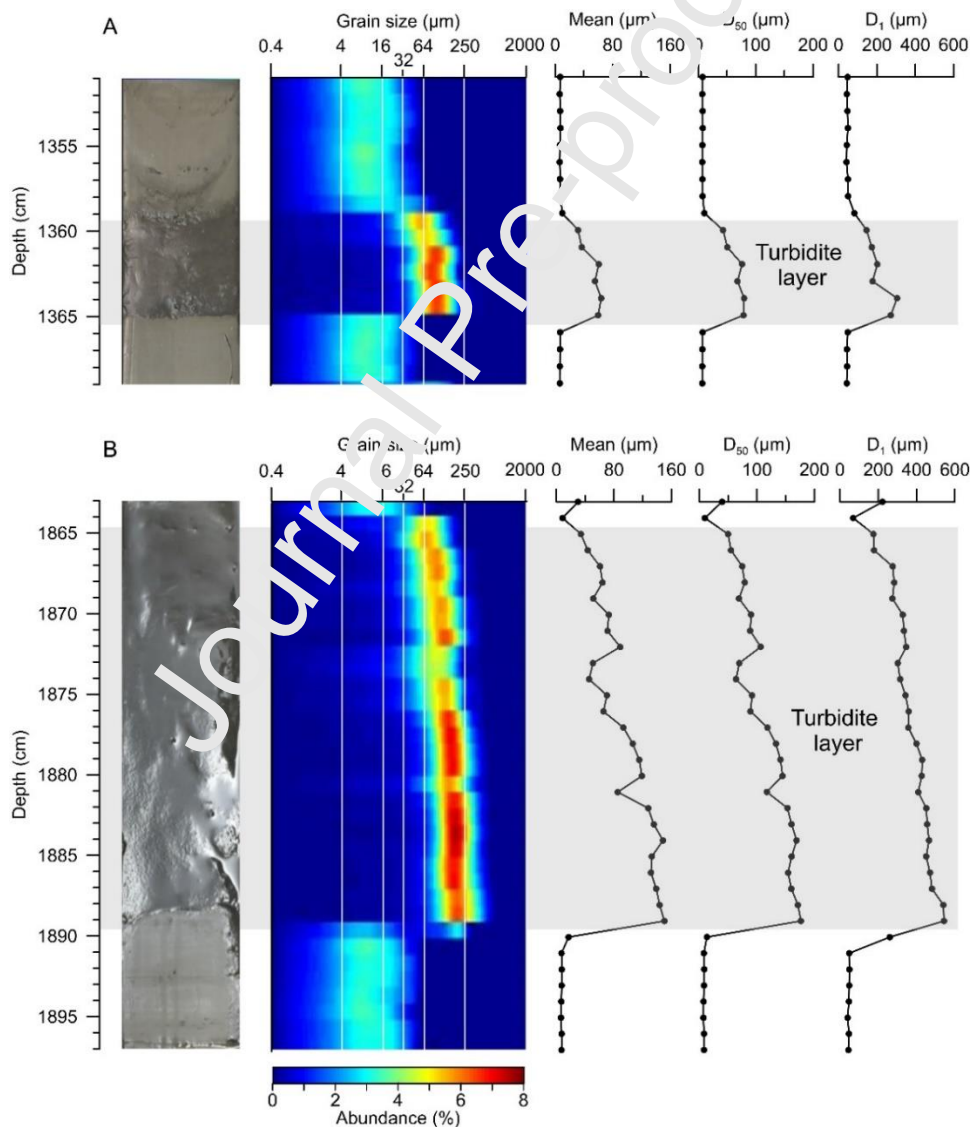showed on their core photos (Fig. 8).

Fig. 8. Grain size distributions of two typical turbidite layers of Core MD18-3565 in the Gaoping

Submarine Canyon, showing core photos, grain-size frequency abundances, and grain-size values of mean,

D_{50} and D_1. (A) A sandy silt layer (depth interval 13.51–13.69 m). (B) A silty sand layer (depth interval

18.63–18.97 m).

5. Discussion

5.1. Turbidity current origin of coarse-grained layers

Basal erosion surface and fining-upward trend of grain size are characteristic of classic Bouma-type

turbidite sequences (Allen, 1991; Middleton, 1993). The lithology-based visual observation shows that all

318 coarse-grained layers at Core MD18-3565 have such turbidite characteristics (Fig. 2). The typical

sandy silt layer and silty sand layer present clear upward fining trends in all grain size values (mean, D_{50},

and D_1), e.g., gradually from coarse to fine silts for the sandy silt layer (Fig. 8A) or from fine sand to fine

silt for the silty sand layer (Fig. 8B) in mean values. The erosion surface at the bottom of the coarse-grained

layers is also very clear, jumping from background mud to coarse-grained silt or fine sand (Fig. 8). Further,

in the *C-M* plot, all samples of the typical sandy silt layer and silty sand layer cluster in a zone, which is

approximately parallel to the *C-M* baseline (Fig. 9). All these grain-size characteristics verify that the

coarse-grained layers at Core MD18-3565 originate from turbidity current activities.
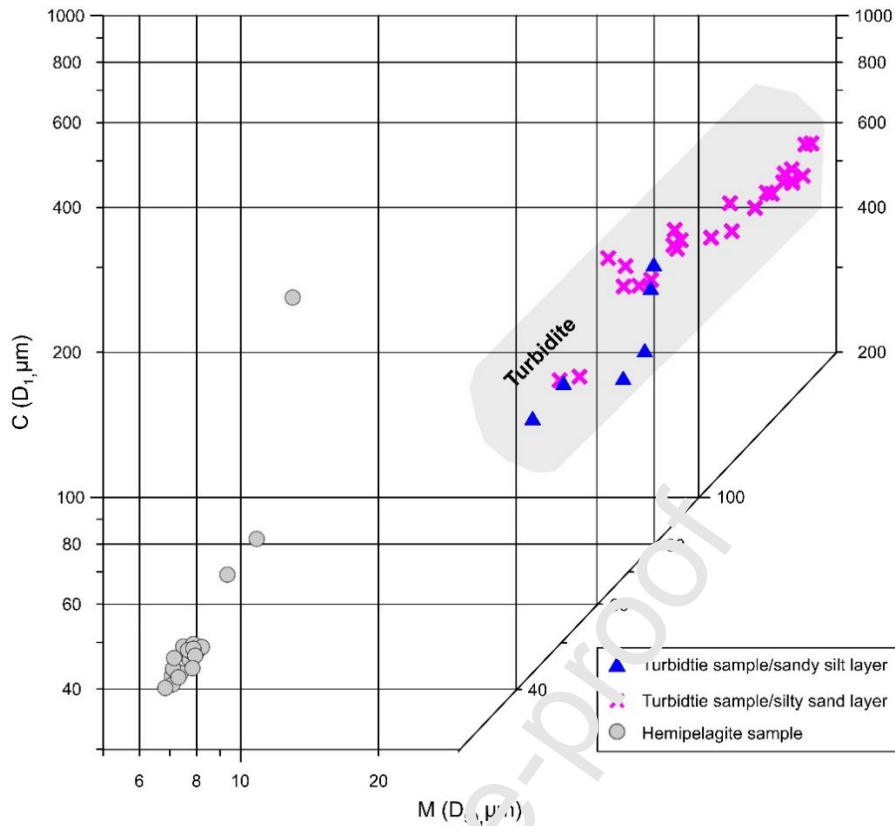
Fig. 9. Grain size *C-M* plot of two typical turbidite layers of Core MD18-3565 in the Gaoping Submarine

Canyon, showing their classic turbidite distributions. Data of the plot are same as in Fig. 8. Note that a

deviated "hemipelagite" sample (*C* = 260 μm, *M* = 12.98 μm) is a mixture of turbidite sand and

hemipelagite mud at the bottom of silty sand layer (Fig. 8B), resulting from the 1-cm sampling resolution.

5.2. Provenance of clay minerals

Previous studies have suggested that the terrigenous sediments in the northeastern SCS are mainly

sourced from fluvial sediments of South China (Pearl River), Taiwan, and Luzon (Liu et al., 2008, 2010;

Chen et al., 2017; Zhao et al., 2018). Clay minerals of Pearl River sediments are composed mainly of

kaolinite (average 47%), and to a lesser extent, illite (34%) and chlorite (18%) (Liu et al., 2007). Fluvial

sediments from Taiwan rivers are abundant in illite (54%) and chlorite (38%) (Liu et al., 2008, 2010; Nayak

et al., 2021). Sediments from western rivers of Luzon are dominated by smectite (87%), with minor

amounts of chlorite (7%) and kaolinite (5%) (Liu Z et al., 2009). The ternary plot of clay mineral

assemblage of Core MD18-3565, along with that of the potential sources, indicates that Core MD18-3565

falls absolutely in the range of Taiwan rivers, implying that the overwhelming majority of, if not all,

terrigenous sediments in the Gaoping Submarine Canyon are sourced from Taiwan (Fig. 10A). The absence

of secular trend in variability of clay mineral contents suggests that the sediment sources have kept almost

unchanged over the late Holocene.

Despite the likeness of clay minerals of riverine sediments from southwest Taiwan, slight differences

among various rivers still exist. Sediments from the Erhjen, Tsengwen, and Pachang rivers have higher

contents of kaolinite (7–13%) and smectite (8–17%) than those of the Linpien, Tungkang, and Gaoping

rivers (kaolinite: 1–3%; smectite: 0–1%; Liu et al., 2008, 2010). Clay mineral assemblage of the turbidites

falls in the range of the Linpien, Tungkang, and Gaoping rivers (Fig. 10B, C), implying that all those rivers

have the potentials to supply sediments to turbidites in the Gaoping Submarine Canyon. Considering that

sediment discharges of the Linpien and Tungkang rivers are 1–2 order of magnitude less than that of the

Gaoping river, the Gaoping river is considered the most prominent source for turbidites in the Gaoping

Submarine Canyon (Table 1). This can also explain the high similarity of illite crystallinity between

samples collected from Core MD18-3565 turbidites and from the Gaoping river (Fig. 11).
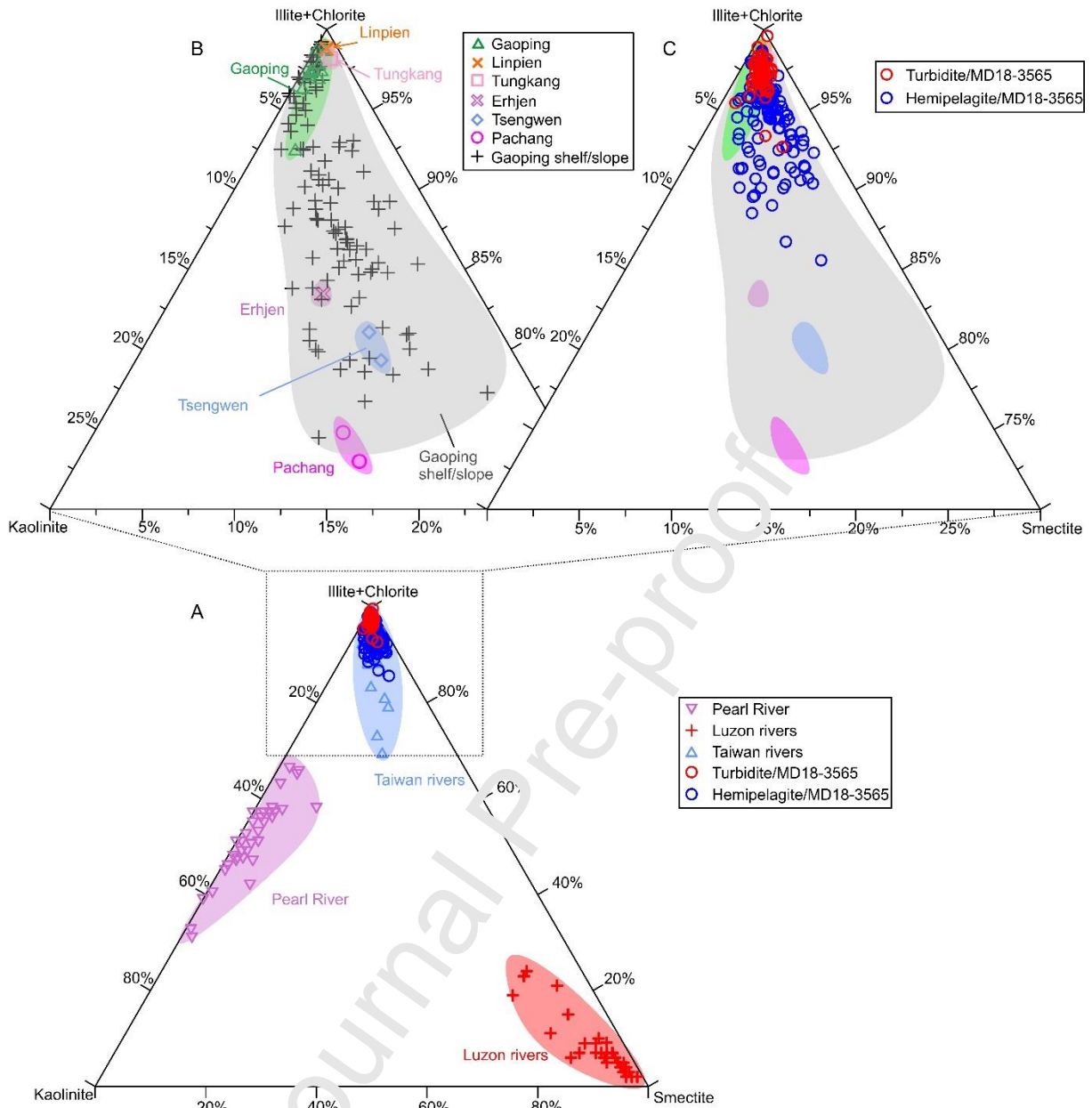
Fig. 10. Ternary diagrams of major mineral groups of illite+chlorite, kaolinite, and smectite. (A) Plots of

turbidite and hemipelagite samples of Core MD18-3565. Clay mineral compositions of surface sediments

from Taiwan rivers, Luzon rivers, and the Pearl River are included for comparison (Liu Z et al., 2008, 2010,

2016). Square in this panel is zoomed in the panels B and C. (B) Zoomed plots for surface sediments of

Taiwan rivers and on Gaoping shelf/slope off southwest Taiwan (Liu Z et al., 2008, 2010, 2016; Nayak et

al., 2021). Note that clay mineral compositions of sediment samples from Gaoping, Linpien, and Tungkang

rivers are very close to the illite+chlorite end-member, while those of sediments from Erhjen, Tsengwen,

and Pachang rivers and Gaoping shelf/slope extend toward kaolinite and smectite end-members. (C)

Comparison of clay mineral assemblages of turbidite and hemipelagite samples of Core MD18-3565 with

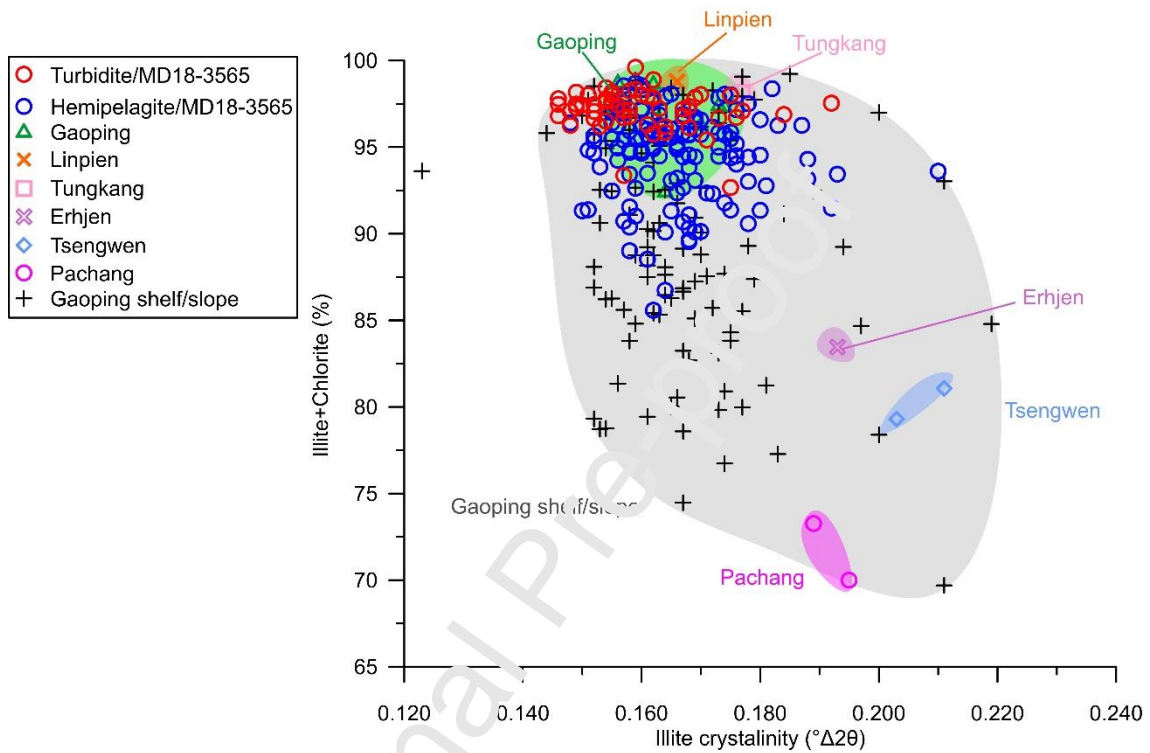those of Taiwan river and Gaoping shelf/slope sediments.

Fig. 11. Contents of illite + chlorite versus illite crystallinity for sediments of Core MD18-3565, and their

comparison with Taiwan river and Gaoping shelf/slope sediments (Liu Z et al., 2008, 2010, 2016; Nayak et

al., 2021).

The clay mineral assemblage of the hemipelagites in Core MD18-3565 falls between the Gaoping

river and the Erhjen, Tsengwen, and Pachang rivers (Fig. 10B, C), indicating a multiple end-member

mixing from these sources. The negative correlation between illite and smectite contents implies that they

are from distinct sources (Fig. 7B), while the positive correlation between smectite and kaolinite contents

implies their homogeneity (Fig. 7C). Clay fraction of sediments of Erhjen, Tsengwen and Pachang rivers is

characterized by slightly higher smectite and kaolinite contents. These rivers are then the most likely source areas for smectite and kaolinite of the hemipelagites. The correlation between illite and chlorite is low, because the combined relative content of illite and chlorite in most samples is ~90–100%. In other words, an increase of illite content will lead to a decrease of chlorite content, and vice versa, the so-called "closed-sum effect" or the dilution effect. The illite crystallinity of hemipelagites in Core MD18-3565 generally coincides with that of the Gaoping river, but extends slightly toward the Erhjen, Tsengwen and Pachang rivers (Fig. 11). To sum up, we conclude that clay minerals of the hemipelagites in Core MD18-3565 are mostly derived from the Gaoping, Erhjen, Tsengwen, and Pachang rivers, with illite and chlorite primarily provided by the Gaoping river, while smectite and kaolinite mostly from the Erhjen, Tsengwen, and Pachang rivers.

The Gaoping shelf/slope is a major sink for riverine inputs from Taiwan. The clay minerals from hemipelagites of Core MD18-3565 highly coincide with the Gaoping shelf/slope on the ternary diagram (Fig. 10B, C), implying that the Gaoping Submarine Canyon also receives a significant contribution of sediments from the continental shelf and slope off Taiwan. These sediments can mostly be tracked back to rivers in southwest Taiwan such as the Gaoping, Erhjen, Tsengwen, and Pachang rivers. Sediments accumulated on the shelf and slope can be further delivered to submarine canyons via reworking/migration of sediments by deep-water currents or earthquake-induced slope failures (e.g., Shanmugam, 1997). However, the clay mineral composition of the turbidites in Core MD18-3565 is clearly different from that of the Gaoping shelf/slope sediments (Fig. 10B, C), suggesting that the Gaoping river is the unique source of turbidites in the Gaoping Submarine Canyon during the late Holocene.

5.3. *Response of turbidites to typhoon activities*

In-situ mooring observation in the middle reach of the Gaoping Submarine Canyon shows that turbidity currents in the modern canyon correspond well with peak river runoff triggered by bypassing typhoons, demonstrating the significant role that typhoon plays in triggering of turbidity currents in the Gaoping Submarine Canyon (Zhang et al., 2018). Typhoon-induced heavy rainfall can cause abrupt increases, usually 2–3 orders of magnitude higher than typhoon-free conditions, in runoff and sediment discharge of the Gaoping river. The narrow shelf off southwest Taiwan and short distance between the head of the Gaoping Submarine Canyon and the mouth of the Gaoping river (<1 km) makes it easily for the fluvial sediments to be delivered directly into the canyon head. When a huge amount of riverine sediments enter the canyon in a short period of time, the density gradient between sediments and the ambient fluid makes it easily to form turbidity currents and move along the canyon floor (i.e., hyperpycnal turbidity currents). Turbidity currents usually move very fast (>15 cm/s) and vanish quickly (in hours to days) in the Gaoping Submarine Canyon (Zhang et al., 2018). The turbidity currents slow down when topography becomes gentle or when they encounter barriers. Deposition of sediments occurred in cases when the speeds of turbidity currents are not sufficient to suspend particles. As most sediments in the turbidites are sourced from the Gaoping river, clay mineral assemblage of the turbidites in the Gaoping Submarine Canyon resembles that of the Gaoping river. All turbidite layers tested in Core MD18-3565 present similar clay mineral characteristics, indicating that most turbidity currents in the Gaoping Submarine Canyon since the late Holocene have been triggered by typhoon activities.

The frequency of turbidite occurrence in Core MD18-3565 is a good indicator of turbidity-current activities during the late Holocene. The nominal frequency interval of turbidity currents in the Gaoping Submarine Canyon is 8 events per 100 years (i.e., around one event per 12.5 yr) over the past 4000 yr, similar to the frequency of ENSO activities during the late Holocene (Moy et al., 2002; Fig. 12). There are

two periods with higher frequency of turbidite occurrence (i.e., 600–1400 cal yr BP and 2600–3500 cal yr

BP) (Fig. 12C). They correspond well to two periods of active ENSO events (Fig. 12D). Thicker turbidite

layers are observed during these two periods (Fig. 12A, B). Previous studies have shown that ENSO can

significantly promote the intensity of typhoon activities (Guo and Tan, 2018, 2021) without increasing the

number of typhoons (Wang and Chan, 2002). During ENSO years, typhoons are generated more easterly in

the Western Pacific and thus have sufficient time to strengthen, along with a weaker Walker circulation.

Such a situation has greatly increased the possibility of turbidity-current occurrence in river-connected

submarine canyons.

Frequency of turbidity currents is similar during the two active periods of 2600–3500 cal yr BP and

600–1400 cal yr BP, while ENSO frequency is lower in the former period. It implies that the response of

typhoon activities to ENSO is not linear, or ENSO isn't the sole mechanism responsible for typhoon

variability over the past 4000 yr. Other factors, e.g., the thermal state of the Western Pacific Warm Pool,

also exert certain influences on the typhoon variability in the SCS (Zhou et al., 2019)
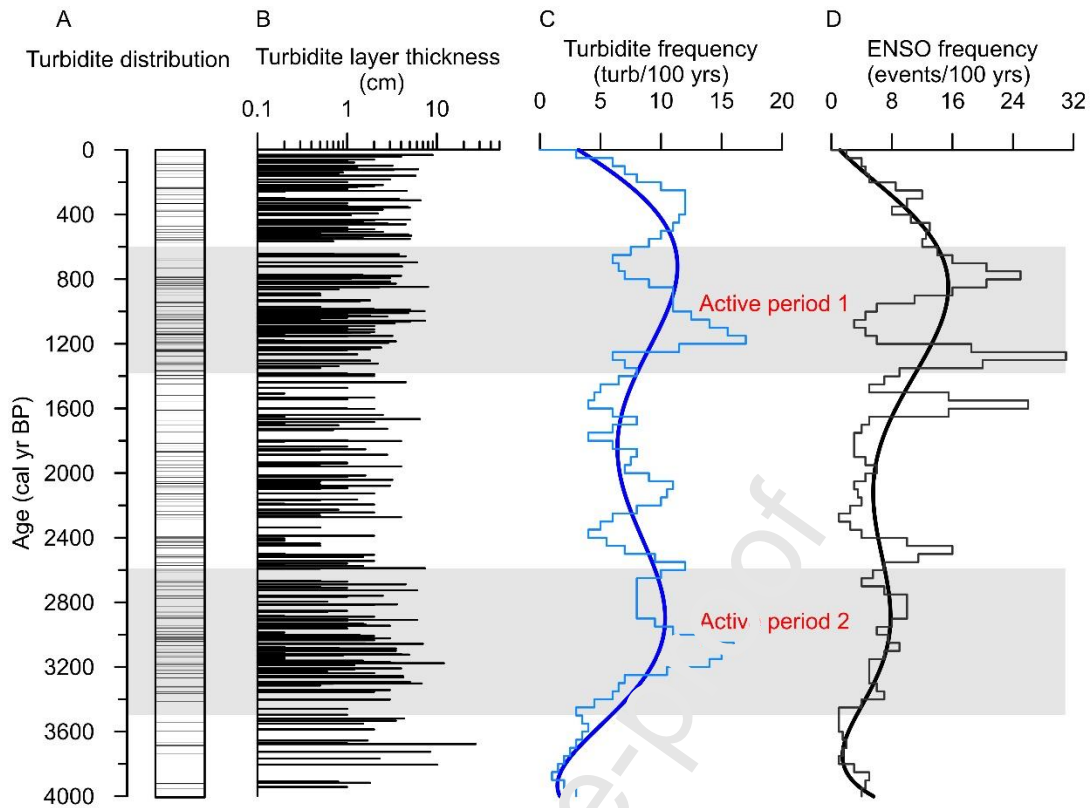
Fig. 12. Frequency of turbidite occurrence at Core MD18-3565 over the past 4000 yr in the Gaoping

Submarine Canyon and its comparison with the temporal variation of ENSO frequency. (A) Turbidite

distribution in the core. (B) Turbidite layer thickness. (C) Turbidite occurrence frequency. (D) ENSO

frequency (Moy et al., 2002). Solid lines in C and D are the polynomial regression trends; shadow bands

identify the strong increase of turbidite occurrence at Core MD18-3565 and referred ENSO frequency.

6. Conclusions

In this study, we have investigated clay mineral assemblages of both turbidites and hemipelagites

combined with grain-size distributions of typical turbidite layers of Core MD18-3565 in the Gaoping

Submarine Canyon at an extremely high temporal resolution. We aim to reconstruct provenance of the

turbidites and to reveal triggering mechanism of the turbidity currents in submarine canyons in the

northeastern SCS over the late Holocene. We conclude that:

(1) High-resolution grain-size analysis of typical coarse-grained layers at Core MD18-3565 shows basal erosion surface and finning-upward trends in all grain size values, along with the *C-M* plot for differentiation, verifying their turbidity current origin.

(2) Clay mineral assemblage of the turbidites in the Gaoping Submarine Canyon indicates that the Gaoping river is the predominant source of the canyon during turbidity-current events, while during non-turbidite periods, the canyon also receives minor contribution of sediments, especially smectite and kaolinite, from the neighboring Erhjen, Tsengwen, and Pachang rivers.

(3) Turbidites in the Gaoping Submarine Canyon have been triggered mostly by sudden increases of sediment inputs from the Gaoping river during the late Holocene, rather than landslides or collapse of sidewall in the canyon. Combining the in-situ observation results, we propose that most of these turbidity currents have been triggered by typhoons passing through Taiwan.

(4) The frequency of turbidites in the Gaoping Submarine Canyon correspond well with variability of the ENSO events, suggesting the potential regulation of ENSO events on long-term changes of typhoon activities in the Western Pacific.

Supplementary data to this article can be found online at http://......

Acknowledgments

References

Allen, J.R.L., 1991. The Bouma division A and the possible duration of turbidity currents. J. Sediment. Res.

61, 291–295.

Biscaye, P.E., 1965. Mineralogy and sedimentation of recent deep-sea clay in the Atlantic Ocean and

adjacent seas and oceans. Geol. Soc. Am. Bull. 76, 803–832.

Blaauw, M., 2010. Methods and code for 'classical' age modelling of radiocarbon sequences. Quat.

Geochronol. 5, 512–518. https://doi.org/10.1016/j.quageo.2010.01.002.

Carter, L., Milliman, J.D., Talling, P.J., Gavey, R., Wynn, R.B., 2012. Near-synchronous and delayed

initiation of long run-out submarine sediment flows from a record-breaking river flood, offshore

Taiwan. Geophys. Res. Lett. 39, L12603. https://doi.org/10.1029/2012GL051172.

Caruso, M.J., Gawarkiewicz, G.G., Beardsley, R.C., 2006. Interannual variability of the Kuroshio intrusion

in the South China Sea. Oceanography 62, 559–575. https://doi.org/10.1007/S10872-006-0076-0.

Chen, J.-M., Li, T., Shih, C.-F., 2010. Tropical cyclone- and monsoon-induced rainfall variability in Taiwan.

J. Clim. 23, 4107–4120. https://doi.org/10.1175/2010JCLI3355.1.

Chen, Q., Liu, Z., Kissel, C., 2017. Clay mineralogical and geochemical proxies of the East Asian summer

monsoon evolution in the South China Sea during Late Quaternary. Sci. Rep. 7, 42083.

https://doi.org/10.1038/srep42083.

Chiang, C.-S., Yu, H.-S., 2006. Morphotectonics and incision of the Kaoping submarine canyon, SW

Taiwan orogenic wedge. Geomorphology 80, 199–213.

https://doi.org/10.1016/j.geomorph.2006.02.008.

Chiang, C.-S., Yu, H.-S., 2011. Sedimentary erosive processes and sediment dispersal in Kaoping

submarine canyon. Sci. China Earth Sci. 54, 259–271. https://doi.org/10.1007/s11430-010-4076-y.

Colin, C., Liu, Z., Lin, A.T.-S., 2018. Report of the Oceanographic Cruise HYDROSED – MD215,

Exploring Paleo-Hydrology and Its Impact on Sedimentary Dynamic Processes in the South China Sea.

R/V MARION DUFRESNE. Orsay (136 pp.).

Commission for the Geological Map of the World, 1975. Geological World Atlas, scale 1:1,00,00,000. UN

Educ. Sci. Cult. Org., Paris.

Dadson, S.J., Hovius, N., Chen, H., Dade, W.B., Hsieh, M.-L., Willett, S.D., Hu, J.-C., Horng, M.-J., Chen,

M.-C., Stark, C. P., Lague, D., Lin, J.-C., 2003. Links between erosion, runoff variability and

seismicity in the Taiwan orogen. Nature 426, 648–651. https://doi.org/10.1038/nature02150.

Fang, G., Fang, W., Fang, Y., Wang, K., 1998. A survey of studies on the South China Sea upper ocean

circulation. Acta. Oceanogr. Taiwanica. 37, 1–16.

Fournier, L., Fauquembergue, K., Zaragosi, S., Zorzi, C., Malaizé, B., Bassinot, F., Joussain, R., Colin, C.,

Moreno, E., Leparmentier, F., 2017. The Bengal fan: External controls on the Holocene active channel

turbidite activity. Holocene 27, 900–913. https://doi.org/10.1177/0959683616675938.

Gavey, R., Carter, L., Liu, J.T., Talling, P.J., Hsu, R., Pope, E., Evans, G., 2017. Frequent sediment density

flows during 2006 to 2015, triggered by competing seismic and weather events: observations from

subsea cable breaks off southern Taiwan. Mar. Geol. 384, 147–158.

https://doi.org/10.1016/j.margeo.2016.06.001.

Gensac, E., 2008. Mise à jour des facteurs de corrections de Biscaye utilisés lors la determination

semi-quantitative de la composition de la fraction argileuse par diffraction des rayons X. Dissertation

for Master's Degree. Université de Lille I, Lille (25 pp.).

Guo, J.H., Underwood, M.B., 2011. Data report: refined method for calculating percentages of kaolinite

and chlorite from X-ray diffraction data, with application to the Nankai margin of southwest Japan. In:

Kinoshita, M., Tobin, H., Ashi, J., Kimura, G., Lallemant, S., Screaton, E.J., Curewitz, D., Masago, H.,

Moe, K.T., Expedition 314/315/316 Scientists. Proc. IODP, 314/315/316: Washington, DC (Integrated

Ocean Drilling Program Management International, Inc.).

https://doi.org/10.2204/iodp.proc.314315316.201.2011.

Guo, Y.-P., Tan, Z.-M., 2018. Westward migration of tropical cyclone rapid-intensification over the

northwestern Pacific during short duration El Niño. Nat. Commun. 9, 1507.

https://doi.org/10.1038/s41467-018-03945-y.

Guo, Y.-P., Tan, Z.-M., 2021. Influence of different ENSO types on tropical cyclone rapid intensification

over the western North Pacific. J. Geophys. Res. Atmos. 126, e2020JD033059.

https://doi.org/10.1029/2020JD033059.

Heaton, T.J., Köhler, P., Butzin, M., Bard, E., Reimer, R.W., Austin, W.E.N., Bronk Ramsey, C., Grootes,

P.M., Hughen, K.A., Kromer, B., Reimer, P.J., Adkins, J., Burke, A., Cook, M.S., Olsen, J., Skinner,

L.C., 2020. Marine20—The marine radiocarbon age calibration curve (0–55,000 cal BP). Radiocarbon

62, 779–820. https://doi.org/10.1017/RDC.2020.68.

Hu, J., Kawamura, H., Hong, H., Qi, Y., 2000. A review on the currents in the South China Sea, seasonal

circulation, South China Sea warm current and Kuroshio intrusion. Oceanography 56, 607–624.

https://doi.org/10.1023/A:1011117531252.

Huang, C.-Y., Wu, W.-Y., Chang, C.-P., Tsao, S., Yuan, P.B., Lin, C.-W., Xia, K.-Y., 1997. Tectonic

evolution of accretionary prism in the arc–continent collision terrane of Taiwan. Tectonophysics 281, 31–35. https://doi.org/10.1016/S0040-1951(97)00157-1.

Kahle, M., Kleber, M., Jahn, R., 2002. Review of XRD-based quantitative analyses of clay minerals in soils: The suitability of mineral intensity factors. Geoderma 109, 191–205. https://doi.org/10.1016/S0016-7061(02)00175-1.

Lin, A.T., Watts, A.B., Hesselbo, S.P., 2003. Cenozoic stratigraphy and subsidence history of the South China Sea margin in the Taiwan region. Basin Res. 15, 453–478. https://doi.org/10.1046/j.1365-2117.2003.00215.x

Liu, J.T., Lin, H.-L., Hung, J.-J., 2006. A submarine canyon conduit under typhoon conditions off southern Taiwan. Deep Sea Res. Part I Oceanogr. 53, 223–240. https://doi.org/10.1016/j.dsr.2005.09.012.

Liu, J.T., Hung, J.-J., Lin, H.-L., Huh, C.-A., Lee, C.-L., Hsu, R.T., Huang, Y.-W., Chu, J.C., 2009. From suspended particles to strata: The fate of terrestrial substances in the Gaoping (Kaoping) submarine canyon. J. Mar. Syst. 76, 417–432. https://doi.org/10.1016/j.jmarsys.2008.01.010.

Liu, J.T., Wang, Y.-H., Yang, R.J., Hsu, R.T., Kao, S.-J., Lin, H.-L., Kuo, F.H., 2012. Cyclone-induced hyperpycnal turbidity currents in a submarine canyon. J. Geophys. Res. Oceans 117, C04033. https://doi.org/10.1029/2011JC007630.

Liu, J.T., Kao, S.-J., Huh, C.-A., Hung, C.-C., 2013. Gravity flows associated with flood events and carbon burial: Taiwan as instructional source area. Ann. Rev. Mar. Sci. 5, 47–68. https://doi.org/10.1146/annurev-marine-121211-172307.

Liu, J.T., Hsu, R.T., Hung, J.-J., Chang, Y.-P., Wang, Y.-H., Rendle-Bühring, R.H., Lee, C.-L., Huh, C.-A., Yang, R.J., 2016. From the highest to the deepest: The Gaoping river–Gaoping submarine canyon dispersal system. Earth-Sci. Rev. 153, 274–300. https://doi.org/10.1016/j.earscirev.2015.10.012.

Liu, Z., Trentesaux, A., Clemens, S.C., Colin, C., Wang, P., Huang, B., Boulay, S., 2003. Clay mineral

assemblages in the northern South China Sea: Implications for East Asian monsoon evolution over the

past 2 million years. Mar. Geol. 201, 133–146. https://doi.org/10.1016/S0025-3227(03)00213-5.

Liu, Z., Colin, C., Trentesaux, A., Blamart, D., Bassinot, F., Siani, G., Sicre, M.-A., 2004. Erosional history

of the eastern Tibetan Plateau since 190 kyr ago: Clay mineralogical and geochemical investigations

from the southwestern South China Sea. Mar. Geol. 209, 1–18.

https://doi.org/10.1016/j.margeo.2010.08.010.

Liu, Z., Colin, C., Huang, W., Le, K.P., Tong, S., Chen, Z., Trentesaux, A., Chen, J., 2007. Climatic and

tectonic controls on weathering in south China and Indochina Peninsula: Clay mineralogical and

geochemical investigations from the Pearl, Red, and Mekong drainage basins. Geochem. Geophys.

Geosyst. 8, Q05005. https://doi.org/10.1029/2006GC001490.

Liu, Z., Tuo, S., Colin, C., Liu, J.T., Huang, C.-Y., Selvaraj, K., Chen, C.-T. A., Zhao, Y., Siringan, F.P.,

Boulay, S., Chen, Z., 2008. Detrital fine-grained sediment contribution from Taiwan to the northern

South China Sea and its relation to regional ocean circulation. Mar. Geol. 255, 149–155.

https://doi.org/10.1016/j.margeo.2008.08.003.

Liu, Z., Zhao, Y., Colin, C., Siringan, F.P., Wu, Q., 2009. Chemical weathering in Luzon, Philippines from

clay mineralogy and major-element geochemistry of river sediments. Appl. Geochem. 24, 2195–2205.

https://doi.org/10.1016/j.apgeochem.2009.09.025.

Liu, Z., Colin, C., Li, X., Zhao, Y., Tuo, S., Chen, Z., Siringan, F.P., Liu, J.T., Huang, C.-Y., You, C.-F.,

Huang, K.-F., 2010. Clay mineral distribution in surface sediments of the northeastern South China

Sea and surrounding fluvial drainage basins: source and transport. Mar. Geol. 277, 48–60.

https://doi.org/10.1016/j.margeo.2010.08.010.

Liu, Z., Zhao, Y., Colin, C., Stattegger, K., Wiesner, M.G., Huh, C.-A., Zhang, Y., Li, X.,

Sompongchaiyakul, P., You, C.-F., Huang, C.-Y., Liu, J.T., Siringan, F.P., Le, K.P., Sathiamurthy, E.,

Hantoro, W.S., Liu, J., Tuo, S., Zhao, S., Zhou, S., He, Z., Wang, Y., Bunsomboonsakul, S., Li, Y.,

2016. Source-to-sink transport processes of fluvial sediments in the South China Sea. Earth-Sci. Rev.

153, 238–273. https://doi.org/10.1016/j.earscirev.2015.08.005.

Liu, Z., Zhang, Y., Zhao, Y., 2020. In situ observation of submarine storms. Sci. & Tech. Rev. 38, 26–29.

https://doi.org/10.3981/j.issn.1000-7857.2020.18.003.

Lombo Tombo, S., Dennielou, B., Berné, S., Bassetti, M.-A., Toucanne, S., Jorry, S.J., Jouet, G., Fontanier,

C., 2015. Sea-level control on turbidite activity in the Rhone canyon and the upper fan during the Last

Glacial Maximum and Early Deglacial. Sediment. Geol. 323, 148–166.

https://doi.org/10.1016/j.sedgeo.2015.04.009.

Middleton, G.V., 1993. Sediment deposition from turbidity currents. Annu. Rev. Earth Planet. Sci. 21, 89–

114.

Milliman, J.D., Farnsworth, K.L., 2011. River Discharge to the Coastal Ocean: A Global Synthesis.

Cambridge University Press, Cambridge (384 pp.).

Moy, C.M., Seltzer, G.O., Rodbell, D.T., Anderson, D.M., 2002. Variability of El Nino/Southern Oscillation

activity at millennial timescales during the Holocene epoch. Nature 420, 162–165.

https://doi.org/10.1038/nature01194.

Nayak, K., Lin, A.T.-S., Huang, K.-F., Liu, Z., Babonneau, N., Ratzov, G., Pillutla, R.K., Das, P., Hsu,

S.-K., 2021. Clay-mineral distribution in recent deep-sea sediments around Taiwan: Implications for

sediment dispersal processes. Tectonophysics 814, 228974.

https://doi.org/10.1016/j.tecto.2021.228974.

Petschick, R., 2000. MacDiff 4.2.2. http://servermac.geologie.un-frankfurt.de/Rainer.html.

Piper, D.J.W., Normark, W.R., 2009. Processes that initiate turbidity currents and their influence on

turbidites: a marine geology perspective. J. Sediment. Res. 79, 347–362.

https://doi.org/10.2110/jsr.2009.046.

Qu, T., Girton, J.B., Whitehead, J.A., 2006. Whitehead J. Deepwater overflow through Luzon Strait. J.

Geophys. Res. Oceans 111, C01002. https://doi.org/10.1029/2005JC003139.

Shanmugam, G., 1997. The Bouma Sequence and the turbidite mind set. Earth-Sci. Rev. 42, 201–229.

https://doi.org/10.1016/S0012-8252(97)81858-2.

Stuiver, M., Reimer, P.J., 1993. Extended ^{14}C database and revised CALIB 3.0 ^{14}C age calibration program.

Radiocarbon 35, 215–230. https://doi.org/10.1017/S0033822200013904.

Su, C.-C., Tseng, J.-Y., Hsu, H.-H., Chiang, C.-S., Yu, H.-S., Lin, S., Liu, J.T., 2012. Records of submarine

natural hazards off SW Taiwan. Geol. Soc. Spec. Publ. 361, 41–60. https://doi.org/10.1144/SP361.5.

Wang, B., Chan, J.C., 2002. How strong ENSO events affect tropical storm activity over the western North

Pacific. J. Clim. 15, 1643–1658.

https://doi.org/10.1175/1520-0442(2002)015<1643:HSEEAT>2.0.CO;2.

Wang, Y., Ren, M.-E., Zhu, D., 1986. Sediment supply to the continental shelf by the major rivers of China.

J. Geol. Soc. 143, 935–944. https://doi.org/10.1144/gsjgs.143.6.0935.

Webster, P.J., 1994. The role of hydrological processes in ocean–atmosphere interactions. Rev. Geophys. 32,

427–476. https://doi.org/10.1029/94RG01873.

Yu, S.-W., Tsai, L.L., Talling, P.J., Lin, A.T., Mii, H.-S., Chung, S.-H., Horng, C.-S., 2017. Sea level and

climatic controls on turbidite occurrence for the past 26 kyr on the flank of the Gaoping canyon off

SW Taiwan. Mar. Geol. 392, 140–150. https://doi.org/10.1016/j.margeo.2017.08.011.

Zhang, Y., Liu, Z., Zhao, Y., Colin, C., Zhang, X., Wang, M., Zhao, S., Kneller, B., 2018. Long-term in situ

observations on typhoon-triggered turbidity currents in the deep sea. Geology 46, 675–678.

https://doi.org/10.1130/G45178.1.

Zhao, S., Liu, Z., Colin, C., Zhao, Y., Wang, X., Jian, Z., 2018. Responses of the East Asian summer

monsoon in the low-latitude South China Sea to high-latitude millennial-scale climatic changes during

the Last Glaciation: Evidence form a high-resolution clay mineralogical record. Paleoceanogr.

Paleoclimatol. 33, 2017PA003235. https://doi.org/10.1029/2017PA003235.

Zhao, Y., Liu, Z., Colin, C., Xie, X., Wu, Q., 2011. Turbidite deposition in the southern South China Sea

during the Last Glacial: Evidence from grain-size and major elements records. Chin. Sci. Bull. 56,

3558–3565. https://doi.org/10.1007/s11434-011-4697-7.

Zhou, L., Yang, Y., Wang, Z., Jia, J., Mao, L., Li, Z., Fang, X., Gao, S., 2019. Investigating ENSO and

WPWP modulated typhoon variability in the South China Sea during the mid–late Holocene using

sedimentological evidence from southeastern Hainan Island, China. Mar. Geol. 416, 105987.

https://doi.org/10.1016/j.margeo.2019.105987.

Declaration of interests

The authors declare that they have no known competing financial interests or personal

relationships that could have appeared to influence the work reported in this paper.

Highlights

- Turbidites in Gaoping Submarine Canyon mainly come from Gaoping river in SW Taiwan.

- Turbidity currents triggered by typhoons are responsible for turbidite occurrence.

- ENSO regulates the occurrence of late Holocene submarine canyon turbidity currents.